Translational Oncology 13 (2020) 100764

Contents lists available at ScienceDirect

Translational Oncology

journal homepage: www.elsevier.com/locate/tranon

Heterogeneous Drug Efficacy of an Antibody-Drug Conjugate Visualized Using Simultaneous Imaging of Its Delivery and Intracellular Damage in Living Tumor Tissues

Kohsuke Gonda [a,*], Hiroshi Negishi [b], Mayumi Takano-Kasuya [a], Narufumi Kitamura [a], Naoko Furusawa [b], Yasushi Nakano [b], Yoh Hamada [c], Masayuki Tokunaga [a], Hideo Higuchi [d], Hiroshi Tada [e], Takanori Ishida [e]

[a] Department of Medical Physics, Graduate School of Medicine, Tohoku University, Sendai, Miyagi 980-8575, Japan
[b] Bio Systems Development Group, Bio Advanced Technology Division, Corporate R&D Headquarters, KONICAMINOLTA. INC., Hino, Tokyo, 191-8511, Japan
[c] Department of Gastroenterological Surgery, Graduate School of Medicine, Tohoku University, Sendai, Miyagi 980-8574, Japan
[d] Department of Physics, Graduate School of Science, University of Tokyo, Tokyo 113-0033, Japan
[e] Department of Breast and Endocrine Surgical Oncology, Graduate School of Medicine, Tohoku University, Sendai, Miyagi 980-8574, Japan

ARTICLE INFO

Article history:
Received 26 November 2019
Accepted 16 March 2020
Available online xxxx

ABSTRACT

Anticancer drug efficacy varies because the delivery of drugs within tumors and tumor responses are heterogeneous; however, these features are often more homogenous *in vitro*. This difference makes it difficult to accurately determine drug efficacy. Therefore, it is important to use living tumor tissues in preclinical trials to observe the heterogeneity in drug distribution and cell characteristics in tumors. In the present study, to accurately evaluate the efficacy of an antibody-drug conjugate (ADC) containing a microtubule inhibitor, we established a cell line that expresses a fusion of end-binding protein 1 and enhanced green fluorescent protein that serves as a microtubule plus-end-tracking protein allowing the visualization of microtubule dynamics. This cell line was xenografted into mice to create a model of living tumor tissue. The tumor cells possessed a greater number of microtubules with plus-ends, a greater number of meandering microtubules, and a slower rate of microtubule polymerization than the *in vitro* cells. In tumor tissues treated with fluorescent dye-labeled ADCs, heterogeneity was observed in the delivery of the drug to tumor cells, and microtubule dynamics were inhibited in a concentration-dependent manner. Moreover, a difference in drug sensitivity was observed between *in vitro* cells and tumor cells; compared with *in vitro* cells, tumor cells were more sensitive to changes in the concentration of the ADC. This study is the first to simultaneously evaluate the delivery and intracellular efficacy of ADCs in living tumor tissue. Accurate evaluation of the efficacy of ADCs is important for the development of effective anticancer drugs.

Introduction

Recently, clinical trials for approximately 70 various antibody-drug conjugate (ADC) candidates have been conducted [1]. ADCs are humanized monoclonal antibodies with a high affinity for the extracellular membrane proteins of their target tumor cells and are covalently bound to small molecular compounds with high cytotoxicity [1–3]. Over 60% of the low–molecular weight compounds used in ADCs are inhibitors of microtubule function [1,4]. Microtubules elongate and shorten via tubulin polymerization and depolymerization and regulate a variety of cellular processes, including cell division, intracellular transport, and cell polarity [5,6].

ADCs containing microtubule inhibitors exert two types of effects: antitumor effects induced by the binding of ADCs to target proteins on the tumor cell membrane after drug delivery and intracellular cytotoxic effects via microtubule inhibitors [2]. During the former type, the binding of the antibody portion of the ADC to the target protein mediates functional inhibition of the target molecule(s) and/or antibody-dependent cell cytotoxicity. On the other hand, the cytotoxic effects during the latter type occur when the ADCs bound to target proteins are incorporated into the cell via endocytosis [7–9]. After endocytosis, the ADC is broken down in the endosome or lysosome, and the microtubule inhibitor is released from the vesicles into the cytoplasm. This process results in inhibition of microtubule function, which induces tumor cell apoptosis. Thus, the important factors for the development of ADCs containing microtubule inhibitors are the specificity of the antibody used in the ADC, the extracellular stability of the linker used to bind the antibody to the low molecular weight drug, the timely breakdown of the conjugate once inside the cell, and the effectiveness of the drug in inhibiting microtubules [1,4]. To evaluate the efficacy of ADCs containing microtubule inhibitors, it is important to quantitatively assess the delivery of ADCs to tumor cells and the effects

* Address all correspondence to: Kohsuke Gonda, Department of Medical Physics, Graduate School of Medicine, Tohoku University, Seiryo-machi, Aoba-ku, Sendai 980-8575, Japan.
E-mail address: gonda@med.tohoku.ac.jp. (K. Gonda).

http://dx.doi.org/10.1016/j.tranon.2020.100764

on microtubule inhibition by the drug once it is inside living tumor cells. However, during most ADC development processes, drug activity is usually analyzed via *in vitro* culture to investigate the ability of the drug to shrink tumors using tumor size measurements, to determine the accumulation of drugs in different organs, and to investigate drug retention in the blood [10–13]. However, there have been no investigations that quantitatively evaluated the correlation between the effects of both ADC delivery and microtubule inhibition in living tumor tissues. Due to the inability to directly visualize drug efficacy in tumor cells during the ADC developmental process, the anticancer effect of ADCs varies for each case of cancer that shows expression of the target molecules of the ADCs. For example, an ADC called trastuzumab emtansine (T-DM1) is created by linking the humanized anti-human epidermal growth factor receptor type 2 (HER2) antibody trastuzumab to the microtubule inhibitor emtansine (DM1) via a thioether linker [3,14]. This ADC was approved for use in HER2-positive and inoperable or relapsed breast cancer patients in 2013 [14]. However, even though T-DM1 showed high efficacy against HER2-positive breast cancer, the efficacy was not different from that of trastuzumab alone when used to treat a HER2-positive gastric cancer patient [15,16].

In recent years, advances in fluorescence imaging technology have allowed the visualization of living tumor tissue in mice *in vivo* and *ex vivo* [17–21]. Such quantitative research on pharmacokinetics and drug efficacy has the potential to improve clinical drug efficacy. Tuber et al. reported methods for measuring changes in the accumulation of fluorescent poly (ADP-ribose) polymerase inhibitors in individual tumor cells over time using the mammalian intravital window [22]. To investigate the efficacy of photoswitchable microtubule inhibitors, Borowiak et al. administered the drug to mice, photoirradiated the mice, then excised tumor tissues, fixed the tissues in formalin, and visualized microtubules by immunostaining with an α-tubulin antibody [23]. Although both approaches are superior technologies, these methods can measure only either the effect of drug delivery to the tumor or its efficacy inside tumor cells.

Furthermore, when evaluating the antitumor efficacy of microtubule inhibitor-containing ADCs, it is important to visualize microtubule dynamics to determine the true drug efficacy in living tumor cells, as microtubules can elongate and shorten due to polymerization and depolymerization [24,25]. Additionally, tumor blood vessels, which are responsible for drug delivery to tumor tissue, are not uniformly distributed, and the availability of oxygen and nutrients is not homogenous throughout the tumor [19]. Therefore, tumor cells have differing expression levels of the ADC target molecule, which result in a heterogeneous distribution of the drug [26–28]. For the reasons stated above, to evaluate the efficacy of microtubule inhibitor-containing ADCs, it is important to visualize tumor cells from multiple regions and to analyze the heterogeneity in the distribution of the drug in living tumors. However, previous research has not identified a method for evaluating the inhibitory effect of ADCs on microtubule dynamics in tumor cells from a wide variety of living tumor tissues, and therefore, it has been difficult to validate such a mechanism with high certainty [10,11,27].

In this study, we introduced a gene that encodes end-binding protein 1 (EB1) fused to enhanced green fluorescent protein (EGFP) (EB1-EGFP) into human breast cancer cells with high HER2 expression [25,29,30]. As EB1-EGFP is a protein that specifically accumulates at the plus-end of microtubules, EB1-EGFP and HER2-expressing cells are useful for visualizing and quantifying HER2-specific T-DM1 delivery and the microtubule inhibition caused by the DM1 contained in T-DM1. First, we analyzed the concentration-dependent microtubule inhibitory effect of T-DM1 by tracking EB1-EGFP kinetics *in vitro* (Figure 1). Next, we tagged T-DM1 with Cy5, a fluorescent dye (Cy5-T-DM1), and then administered the Cy5-T-DM1 via the mouse tail vein to analyze its efficacy in living tumor tissue (Figure 1). After delivery of the Cy5-T-DM1 to the tumor, a 200-μm–thick section of the living tumor was prepared, and the Cy5-T-DM1 efficacy was determined *ex vivo* using fluorescence imaging (Figure 1). For the control groups, to which Cy5-T-DM1 was not administered, the number of elongated microtubule ends was greater, and the microtubules elongated more slowly and meandered more in the living tumor tissues than in cells cultured *in vitro*; thus, the microtubules exhibited distinctive features associated with tumors. After observing these features of microtubules in living tumors, we visualized the delivery of T-DM1 to tumors and the microtubule dynamics in living tumor cells via fluorescence imaging, showing that we are the first group to successfully and simultaneously visualize the heterogeneity of T-DM1 drug delivery in a tumor and its effect on the inhibition of microtubule elongation inside single tumor cells (Figure 1).

Materials and Methods

Construction and Culture of EB1-EGFP Gene-Expressing Cancer Cells

To generate an EB1-EGFP gene construct, the open reading frame of human EB1 cDNA was amplified from a human cDNA pool and inserted into a pEGFP cloning vector (TaKaRa Bio Inc.). The excised EB1-EGFP cDNA sequence was inserted into a pLNCX2 retroviral vector (BD Bioscience). The human KPL-4 breast cancer cell line was kindly provided by Dr. J. Kurebayashi (Kawasaki Medical School, Japan) [31]. EB1-EGFP–expressing KPL-4 cells (EB1-EGFP-KPL cells) were created by transducing KPL-4 cells using the pLNCX2 retroviral vector system containing the EB1-EGFP gene as the insert, and the cells were then cloned. The cloned EB1-EGFP-KPL cells were cultured in Dulbecco's modified Eagle medium (DMEM) (Thermo Fisher Scientific) containing 10% fetal bovine serum and 400 μg/ml G418 (Thermo Fisher Scientific) at 37°C with 5% CO_2.

Purification of Antibody Drugs and Their Fluorescence Labeling

Kadcyla (T-DM1) (Chugai Pharmaceutical, Japan) and Herceptin (trastuzumab) (Chugai Pharmaceutical) were used as antibody drugs. T-DM1 and trastuzumab were diluted in 100 mM 4-(2-hydroxyethyl)-1-piperazineethanesulfonic acid buffer containing 30% glycerol and purified using ultrafiltration filters (NanoSep 30K; Pall). Purified T-DM1 and trastuzumab concentrations were measured at a wavelength of 280 nm using an absorption spectrometer (NanoDrop; Thermo Fisher Scientific).

The Cy5 labeling of antibodies was performed using an amine biotin kit (DOJINDO, Japan), with Cy5 mono N-hydroxysuccinimide (NHS) ester (GE Healthcare) used in place of the NHS biotin included in the kit. A 10-μl sample of Cy5 mono NHS ester diluted to a concentration of 8.5 mM was added to 100 μg (1 mg/ml) of antibody drug in dimethyl sulfoxide and incubated at 37°C for 15 minutes. The concentrations of the labeled T-DM1 and trastuzumab, as well as the labeling efficiencies (moles of Cy5/moles of antibody), were determined using the NanoDrop spectrophotometer. Protein absorbance was measured at 280 nm, and Cy5 absorbance was measured at 640 nm to calculate their concentrations by using the molar absorption coefficients. We prepared a sample with a Cy5/antibody molar ratio of 3.0 ± 0.3 (mean ± SD). T-DM1 and trastuzumab labeled with Cy5 were named Cy5-T-DM1 and Cy5-trastuzumab, respectively.

Effect of Antibody Drugs on Cell Viability

The effect of T-DM1 and trastuzumab on EB1-EGFP-KPL cell viability was measured using the commercial methyl thiazolyl tetrazolium (MTT) assay (Thermo Fisher Scientific) performed according to the manufacturer's instructions. Briefly, 1.0×10^4 EB1-EGFP-KPL cells were seeded per well in 96-well plates. Purified T-DM1 or trastuzumab was diluted to an arbitrary concentration with FluoroBrite DMEM. Next, the cells in 96-well plates were treated with concentration gradients of the diluted T-DM1 or trastuzumab (10^{-5}-10^2 μg/ml) and allowed to grow for the next 72 hours prior to the measurement of cell viability using the MTT assay in a FlexStation 3 Multi-Mode Microplate Reader (Molecular Devices, Sunnyvale, CA).

In Vitro Imaging

The subcultured EB1-EGFP-KPL cells were seeded at a density of 2×10^4 cells/dish on No. 1.5 35-mm glass-bottomed dishes (MatTek) with a thin coating of Matrigel (Corning) and cultured at 37°C in 5% CO_2. The cells were washed with FluoroBrite DMEM (Thermo Fisher Scientific), a

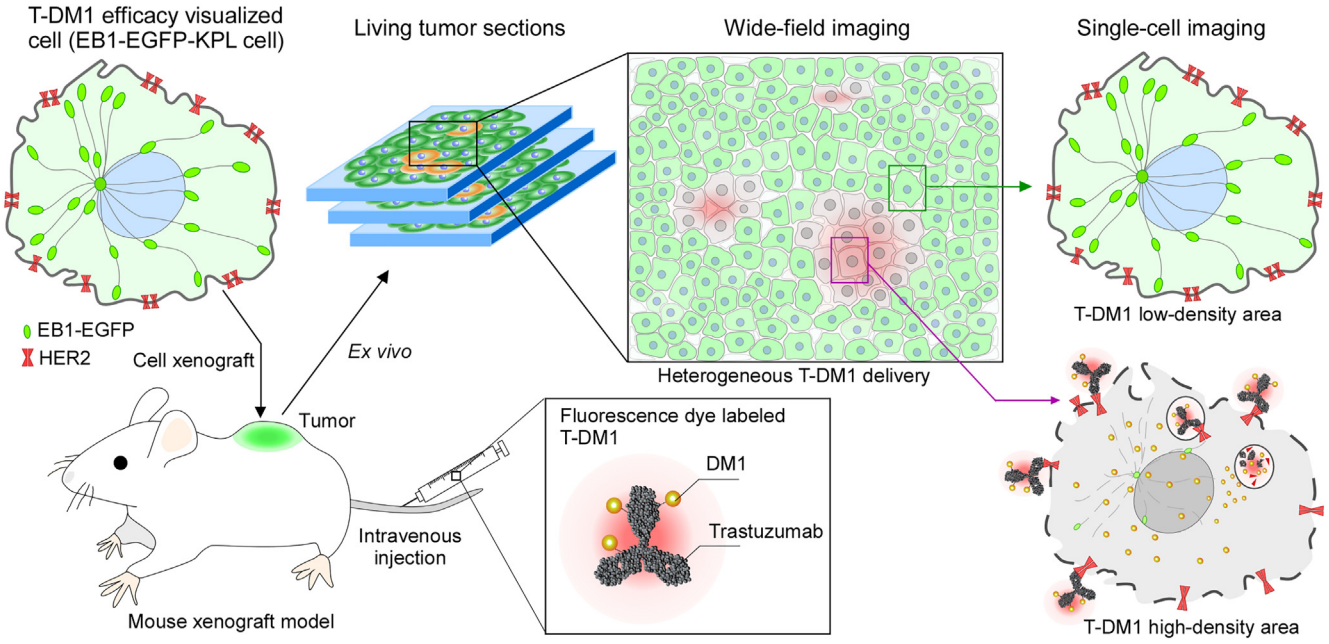

Figure 1. Summary of the research concept. Our research objective was to increase the precision with which the mechanisms of anticancer drug efficacy can be elucidated during preclinical trials, from drug development to clinical application, to increase the success rate of new drug development. To clarify the mechanisms contributing to the efficacy of ADC-containing microtubule inhibitors, it is important that the drug delivery and the effect of the drug on microtubule dynamics are investigated using living tumor tissues. In this study, we simultaneously visualized the effects of T-DM1 drug delivery and the inhibition of microtubule elongation in a living tumor environment, as opposed to an *in vitro* or fixed tissue environment. We then analyzed the data quantitatively and in an integrated manner. This method is hypothesized to demonstrate drug efficacy in a method that is unique to the tumor environment. We subcutaneously xenografted a cell line with high HER2 expression, transformed with an EB1-EGFP gene to visualize T-DM1 efficacy in cells, into immunodeficient mice to create a tumor-bearing mouse model. T-DM1 labeled with a fluorochrome was injected into the tail vein of these mice and delivered to the tumor due to enhanced permeability and retention effects. After tumor excision, we immediately generated 200-μm–thick living tumor sections from each tumor using a Vibratome and observed the tissues at 37°C using fluorescence imaging. The amount of T-DM1 delivered to tumor cells and the amount of EB1-EGFP comet movement in cancer cells from different parts of the living tumor tissue were imaged simultaneously. Since anticancer drugs are delivered to tumor tissues in a nonhomogeneous manner and tumors are composed of heterogeneous groups of cancer cells, observing different areas of living cancer tissues is an effective method to elucidate the detailed mechanisms of ADC efficacy.

culture medium suited to *in vitro* imaging, and the medium was then changed to FluoroBrite DMEM. EB1-EGFP-KPL cells were observed using an A1R confocal laser microscope system (Nikon). A 60× (NA = 1.40) apochromatic lens was used as the objective lens. A 488-nm laser set to 0.5% output was used as the excitation light source for the observation of EB1-EGFP comet movement. The laser-excited EGFP fluorescence was filtered with a 500-50-nm bandpass filter. A resonant scanner was used as the detector, with an HV of 75 arbitrary units (a.u.), resolution of 512 × 512, and a pixel size of 0.104 μm. Time-lapse imaging was conducted at a scan speed of 1.07 s/frame continuously over 20 seconds.

The effect of antibody drugs without Cy5 on microtubule elongation activity in EB1-EGFP-KPL cells was observed via time-lapse imaging using the optical conditions described above for *in vitro* imaging. When Cy5-T-DM1 and Cy5-trastuzumab were used to examine the effect of these drugs on the microtubule elongation activity in EB1-EGFP-KPL cells, imaging of EB1-EGFP was performed using the same optical method described above. In this case, the Cy5-labeled antibody drug was observed using a 640-nm laser. The laser-excited Cy5 fluorescence was filtered through a 633-738-nm bandpass filter. The resonant scanner was used as the detector for imaging, with an HV of 80 a.u., resolution of 512 × 512, and a pixel size of 0.104 μm. The fluorescence intensity of Cy5 was analyzed using FIJI/ImageJ. To analyze the Cy5 fluorescence intensity in individual cells, the average signal value from the autofluorescence of tumors that were not treated with the Cy5-labeled antibody drug was subtracted from the signal value obtained from the images.

Analysis of EB1-EGFP Comet Movement

To measure the movement of EB1-EGFP comets, the time-lapse images obtained using confocal microscopy were analyzed using Imaris Version 9.1 (Bitplane). The comet-recognition algorithm used was the "track spots (over time)" function. The parameters used were "diameter" of 0.5 μm and "quality" of 10 a.u. "Autoregressive motion" was used for the tracking algorithm, with the "max distance" set to 0.8 μm and the "max gap size" set to three time points. To avoid misrecognition due to image noise in the tracking data, only spots that could be tracked for three or more time points were analyzed.

Animal Experiments

Five- to 6-week-old female immunodeficient mice (BALB-c nu/nu) from Charles River (Japan) were used. To prepare the tumor-bearing mice, 2×10^7 EB1-EGFP-KPL cells were subcutaneously injected into the lumbus of mice. EB1-EGFP-KPL–xenografted mice were housed for 4-5 weeks until the tumor size was 5-10 mm, at which point the specimens were harvested. The animal experiment protocol used in this study was approved by the Tohoku University Animal Ethics Committee.

Administration of Antibody Drugs to Mice and Ex Vivo Imaging

A 200-μl sample of Cy5-labeled antibody-drug diluted to 1.5 mg/ml with saline solution was injected into the tail vein of mice under anesthesia. The mice were euthanized 24 hours after the antibody-drug injection, and the subcutaneous tumors were excised. The excised tumors were washed with FluoroBrite DMEM and placed in a 37°C environment. Next, samples were embedded in low–melting point agarose (PrimeGel 1-20 K, TaKaRa Bio) diluted to 1.5% (w/v) in saline solution. Sections 200 μm in size were prepared using the linear slicer PRO 7 (Dosaka EM, Japan) from the agarose blocks containing the embedded

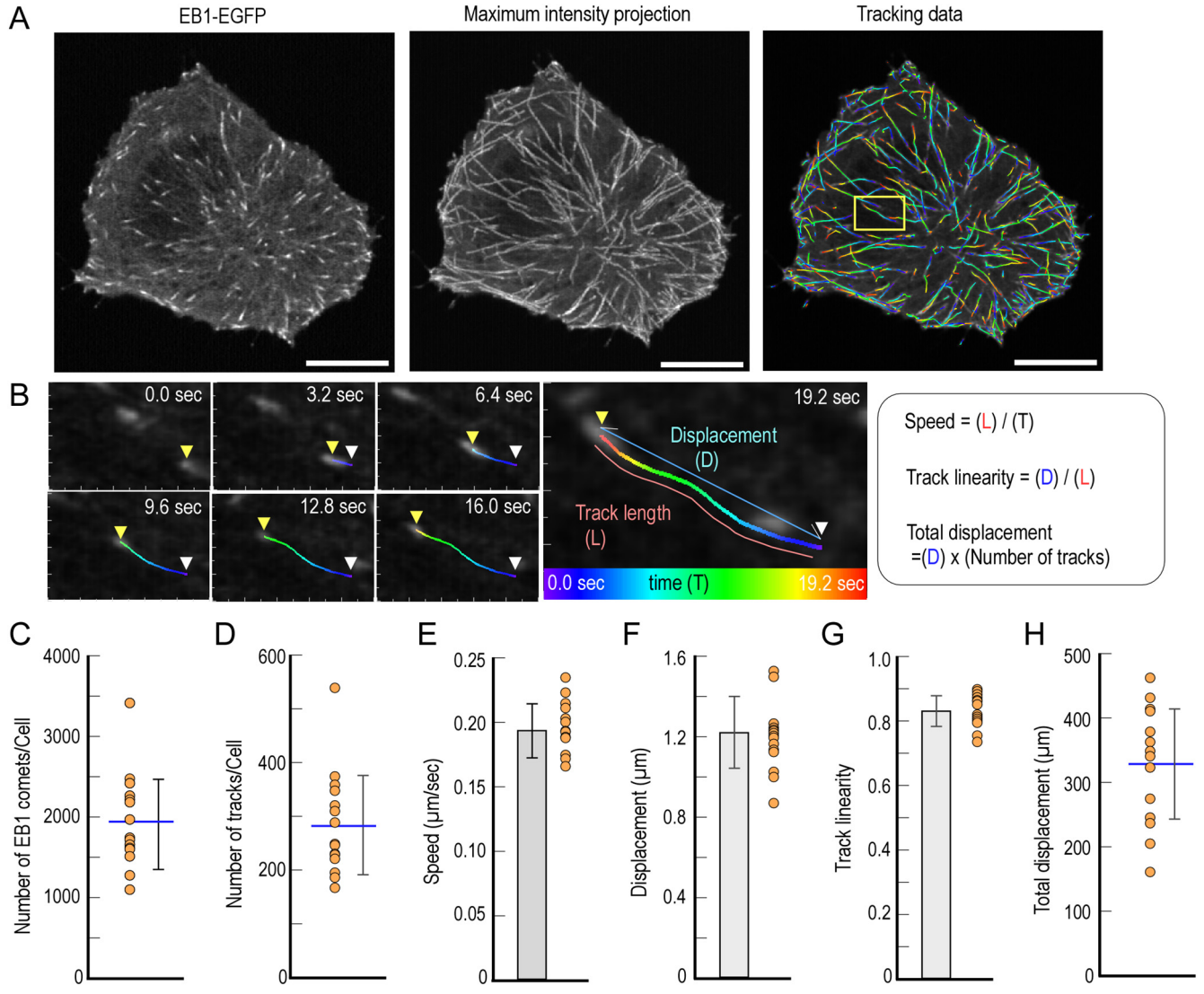

Figure 2. *In vitro* evaluation of microtubule elongation in EB1-EGFP-KPL cells. (A) Typical images of EB1-EGFP-KPL cells obtained using fluorescence imaging and analysis software. The image on the left is a still image with an exposure time of 1.07 seconds. The time-lapse image in the center was created using maximum intensity projection methods to overlay all the fluorescence images. The image on the right shows a digital image of the EB1-EGFP comet movement as measured using the Imaris software. The image is overlaid on top of the center image. The color scale is the same as in B. The yellow square denotes the location of the microtubules that were analyzed in B. Bar, 10 μm. (B) Images of the tracks of the microtubules are shown in the yellow square in A every 3.2 seconds. The images are overlays of the time-lapse fluorescence image and the digital image created using Imaris. The white arrowheads show the locations of the comets at the start of tracking, and the yellow arrowheads show the locations of the comets at the indicated time points. The color scale represents the location of the comets at different time points. (C-H) Analysis results of EB1-EGFP comet movements that could be tracked for at least 2 seconds during the 20-second observation period ($n = 15$). (C) Number of EB1-EGFP comets per cell (orange dots). (D) Number of EB1-EGFP comet tracks per cell (orange dots). (E) Mean speed of EB1-EGFP comets in all cells (bar) and per cell (orange dots). (F) Mean track displacement of EB1-EGFP comets in all cells (bar) and per cell (orange dots). (G) Mean track linearity of EB1-EGFP comets in all cells (bar) and per cell (orange dots). (H) Total track displacement per cell (orange dots). Blue bars and error bars present the average value and SD of EB1-EGFP comets per cell (C, D, H). The error bars indicate the SD of the mean value of EB1-EGFP comets in all cells (E-G).

tumors. The sections were washed using FluoroBrite DMEM and maintained at 37°C. Later, the living tumor tissue sections were placed on a No. 1.5 35-mm glass-bottomed dish with adequate FluoroBrite DMEM and covered with a circular coverslip.

Ex vivo whole tumor tissue imaging of EB1-EGFP and Cy5-T-DM1 or Cy5-trastuzumab was basically performed under the same optical conditions used for the *in vitro* imaging. The pixel size was modified from 0.104 μm to 0.416 μm since we needed many images to obtain a tiling image of the whole tissues. The images for tiling were taken in moving steps, where the images overlapped with each other by 20%. After the images were obtained, they were connected into a single image of whole tumor tissue by using the A1R confocal laser microscope system. Enlarged tumor tissue imaging of EB1-EGFP and Cy5-T-DM1 or Cy5-trastuzumab was performed under identical optical conditions used for *in vitro* imaging.

Statistical Analyses

All data are presented as the mean ± SD. Statistical analyses were performed using Microsoft Excel software. Statistical significance was determined using two-tailed *t* tests or analysis of variance, where appropriate. *P* values of 0.05 were considered significant and are indicated by "*"; *P* values of 0.01 are indicated by "**."

Results

The Inhibitory Effect of T-DM1 on Microtubule Dynamics In Vitro

To visualize the efficacy of T-DM1, we used a retroviral vector to stably integrate the EB1-EGFP gene into KPL-4 cell chromosomal DNA. KPL-4 cells

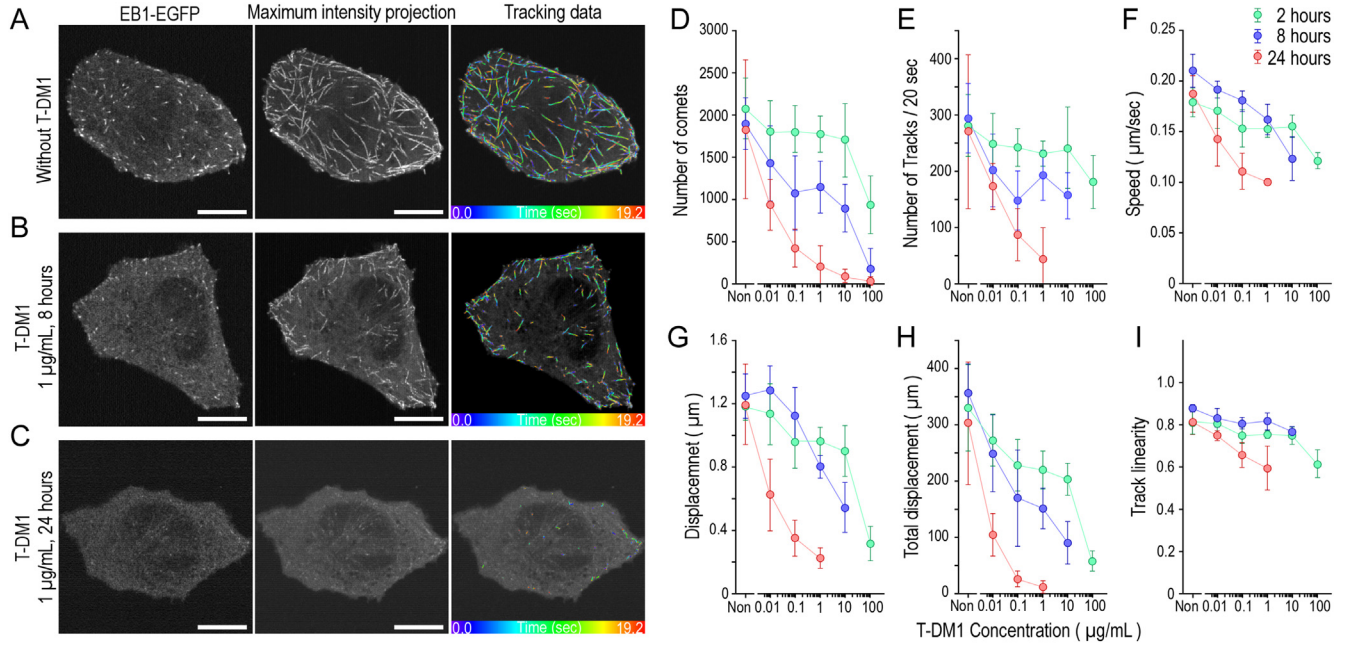

Figure 3. Effect of T-DM1 on microtubule elongation in EB1-EGFP-KPL cells *in vitro*. (A) Typical images of an EB1-EGFP-KPL cell not treated with T-DM1. (B) Typical images of an EB1-EGFP-KPL cell treated with 1 μg/ml T-DM1 for 8 hours. (C) Typical images of an EB1-EGFP-KPL cell treated with 1 μg/ml T-DM1 for 24 hours. In A-C, similar to Figure 2*A*, the image on the left is a still image, the time-lapse image in the center was created using maximum intensity projection methods to overlay all the fluorescence images, and the image on the right is a digital image showing EB1-EGFP comet movement as determined by Imaris, overlaid on top of the center image. Bar, 10 μm. The color scale represents the location of comets at different time points. (D-I) Analysis results of EB1-EGFP comet movement in EB1-EGFP-KPL cells treated with 0, 0.01, 0.1, 1, 10, and 100 μg/ml T-DM1 for 2, 8, and 24 hours. Comet movements that could be tracked for at least 2 seconds during the 20-second observation period were included in the analysis (D-I). Five cells were analyzed for each treatment condition (D-I). (D) Changes in the mean number of EB1-EGFP comets per cell. (E) Change in the mean number of EB1-EGFP comet tracks per cell. (F) Changes in the mean movement speed of all EB1-EGFP comets in five cells. (G) Changes in the mean track displacement of all the EB1-EGFP comets. (H) Changes in the mean total track displacement per cell. (I) Changes in the mean track linearity during movement of all EB1-EGFP comets in five cells. The error bars in D-I represent the SD. In EB1-EGFP-KPL cells treated with 10 μg/ml T-DM1 for 24 hours and 100 μg/ml T-DM1 for 8 or 24 hours, EB1-EGFP comets that could be tracked for 2 seconds or more are rarely observed. Therefore, the data obtained during these conditions are not included in E-I.

are human breast cancer cells with high expression of HER2, the antigen for trastuzumab [10,31,32]. Multiple molecules of EB1-EGFP will bind directly to the plus-end of a microtubule and move in a comet-like fashion during microtubule elongation [29,30,33,34]. As a control experiment, we incubated and observed cloned EB1-EGFP–expressing KPL-4 (EB1-EGFP-KPL) cells at 37°C in the absence of T-DM1. EB1-EGFP accumulated at the ends of elongating microtubules (Figure 2*A*, left image). Next, using an exposure time of 1.07 s/frame with no delay, we performed a 20-second time-lapse image sequence and then overlaid all imaging data. EB1-EGFP comets moving straight towards the cell membrane were observed (Figure 2*A*, middle image; Supplementary Movie S1; Figure 2*B*). The comets shown in the continuous images from the 20-second time-lapse sequence could be tracked for differing lengths of time. Using the analysis software (Imaris), we conducted a bright spot tracking analysis of EB1-EGFP comets and created an overlaid image using all the tracking data (Figure 2*A*, colored portion of the right image), which demonstrated the same results as the fluorescence images in the middle of Figure 2*A*. This finding indicated that our analysis accurately measured EB1-EGFP comets. In 15 arbitrary cells, measurement of the movements of EB1-EGFP comets, as determined using Imaris, demonstrated that for 20 seconds of continuous observation, the total number of comets was 1938.0 ± 557.5/cell (mean ± SD; Figure 2*C*). The comets that were visualized at a specific time point (*t*) were compared with those measured at $t + 1$. Upon joining comets that were within 0.8 μm of each other, 280.7 ± 92.5 tracks/cell were observed for ≥2 seconds (mean ± SD; Figure 2*D*). Based on the tracking data, the average movement speed of all the comets that we tracked for ≥2 seconds was 0.19 ± 0.02 μm/s (mean ± SD; Figure 2, *B* and *E*). These EB1-EGFP localization patterns and movement speeds were similar to those previously measured [34]. Furthermore, for the comets that could be tracked for ≥2 seconds within the 15 arbitrary cells, the total distance traveled was 1.21 ± 0.18 μm/comet (mean ± SD; Figure 2*F*). The track linearity while moving was 0.83 ± 0.05/comet (mean ± SD; Figure 2*G*). The track linearity was calculated by dividing the total linear distance traveled by the distance actually moved; this measurement indicates the degree of meandering in the direction of microtubule elongation (Figure 2*B*, right image). Additionally, the total track displacement over the 20 seconds was 332.3 ± 85.3 μm/cell (mean ± SD; Figure 2*H*).

Next, we treated EB1-EGFP-KPL cells with 1 μg/ml T-DM1 for 8 or 24 hours and then captured 20 seconds of time-lapse images of the cells to evaluate the effect of T-DM1 on microtubule elongation activity in EB1-EGFP-KPL cells *in vitro*. Many EB1-EGFP comets were observed in the control experiment with no T-DM1 treatment (Figure 3*A*; Supplementary Movie S2). However, after treatment with T-DM1 (8 hours, Figure 3*B*; 24 hours, Figure 3*C*), the number of EB1-EGFP comets decreased over time (left images in Figure 3, *B* and *C*), and movement halted (middle images in Figure 3, *B* and *C*; Supplementary Movie S3 and S4). Additionally, a bright spot tracking analysis of EB1-EGFP comets was conducted using Imaris (right images in Figure 3, *B* and *C*). To our knowledge, this is the first study to directly visualize microtubule elongation in cells in response to treatment with a microtubule inhibitor-containing ADC using a microtubule plus-end tracking protein. Furthermore, to analyze the effects of T-DM1 on microtubule elongation in detail, EB1-EGFP-KPL cells were cultured for 2, 8, or 24 hours in the presence of 0, 10^{-2}, 10^{-1}, 1, 10, or 10^{2} μg/ml T-DM1, and the EB1-EGFP comet movements in these cells were quantitatively analyzed. Five arbitrarily selected cells in each treatment group were continuously imaged with a 20-second time-lapse image sequence, and the movement of EB1-EGFP comets

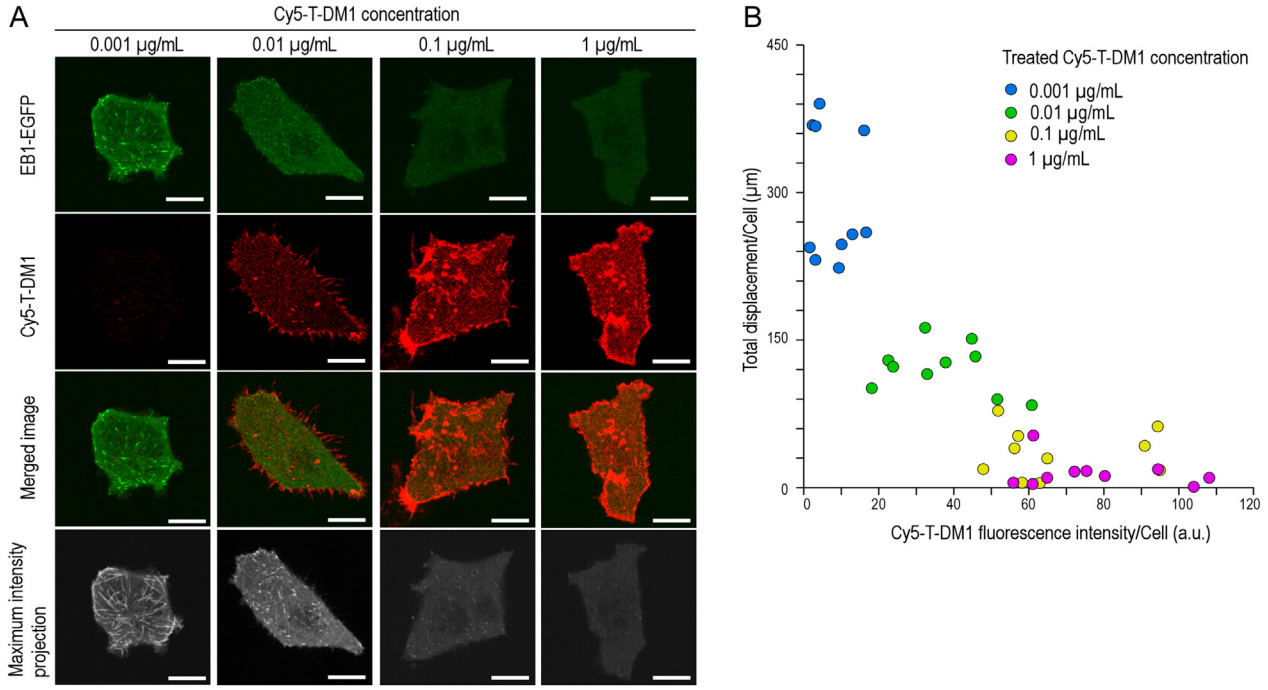

Figure 4. Relationship between the amount of T-DM1 interacting with the EB1-EGFP-KPL cells and the inhibitory effect of T-DM1 on microtubule elongation in the cells *in vitro*. (A) Typical images of EB1-EGFP-KPL cells treated with 0.001 (left column), 0.01 (center left column), 0.1 (center right column), and 1 (right column) μg/ml Cy5-T-DM1 for 24 hours. In each column, fluorescence signal of EB1-EGFP (green, top line), fluorescence signal of Cy5-T-DM1 (red, second line from the top), merged image of EB1-EGFP and Cy5-T-DM1 (third line from the top), and time-lapse image for 20 seconds created using maximum intensity projection methods (bottom line) are shown. (B) The correlation between the amounts of Cy5-T-DM1 delivered to EB1-EGFP-KPL cells and microtubule polymerization activity. The activities in each cell are represented as total displacement/cell (μm). Blue, green, yellow, and pink dots present the conditions treated with 0.001 μg/ml, 0.01 μg/ml, 0.1 μg/ml, and 1 μg/ml Cy5-T-DM1, respectively ($n = 10$). For each image in A, Cy5-T-DM1 fluorescence intensity and total displacement/cell in the cells treated with 0.001, 0.01, 0.1, and 1 μg/ml Cy5-T-DM1 for 24 hours are 6.4 a.u. and 362.6 μm, 43.5 a.u. and 151.0 μm, 89.6 a.u. and 44.0 μm, and 102.8 a.u. and 0.2 μm, respectively (B).

that could be tracked for ≥2 seconds was analyzed in a manner as shown in Figure 2. At all concentrations, the results revealed a time-dependent decrease in the number of comets (Figure 3*D*), the number of tracks that could be tracked (Figure 3*E*), the speed of comets (Figure 3*F*), and the average track displacement (Figure 3*G*) in each cell. Furthermore, the total track displacement over 20 seconds also decreased in a T-DM1 concentration-dependent fashion (Figure 3*H*). However, the differing T-DM1 concentrations and reaction times did not significantly alter track linearity (Figure 3*I*). These results indicated that T-DM1 decreased the appearance of microtubules with elongating ends and the elongation speed of these microtubules throughout the whole cell.

To support the results of the T-DM1 inhibition experiments described above, we treated EB1-EGFP-KPL cells with DM1 alone; the cells exhibited a time-dependent decrease in the number of EB1-EGFP comets similar to that observed during T-DM1 treatment (Supplementary Figure 1). The disappearance of comets and the halting of movement were not observed after treatment with trastuzumab alone (Supplementary Figure 2). Additionally, to investigate these antibody drugs on cell viability, T-DM1 or trastuzumab was incubated in concentration gradients (10^{-5}-10^{2} μg/ml) with EB1-EGFP-KPL cells at 37°C for 72 hours, and MTT assays were performed. The results demonstrated that T-DM1 affects the viability in a concentration-dependent manner; however, trastuzumab did not (Supplementary Figure 3). Therefore, these data suggested that the concentration- and time-dependent inhibition of microtubule elongation by T-DM1 observed in this study resulted due to the DM1 molecule in the T-DM1 complex.

Next, to investigate the relationship between the amount of T-DM1 binding and internalized to the EB1-EGFP-KPL cells and inhibitory effect of T-DM1 on microtubule elongation in the cells, T-DM1was labeled with a fluorescent dye, Cy5 (Cy5-T-DM1), and incubated with the EB1-EGFP-KPL cells. When the cells were treated with 0.001 μg/ml Cy5-T-DM1 for 24 hours, despite a weak fluorescence signal of Cy5-TDM1 detected in the cells, inhibition of microtubule elongation by T-DM1 was not observed (Figure 4*A*, four left panels). On the other hand, during incubation with 0.01 μg/ml (Figure 4*A*, four center-left panels), 0.1 μg/ml (Figure 4*A*, four center-right panels), or 1 μg/ml Cy5-T-DM1 (Figure 4*A*, four right panels), the fluorescence signal of Cy5-TDM1 on and in the cells increased dependent on the Cy5-T-DM1concentration, and the appearance of microtubules with elongating ends decreased in a Cy5-T-DM1 concentration-dependent fashion. As these results (Figure 4*B*) were comparable to the data using nonlabeled T-DM1 (Figure 3*H*, red circles which show the conditions incubated for 24 hours), it was considered that the Cy5 label did not affect T-DM1 activity.

Ex Vivo Imaging of Microtubule Dynamics in Living Tumor Cells Using EB1-EGFP-KPL Cells Transplanted into Tumor-Bearing Mice

The *in vitro* data obtained on microtubule dynamics in the conditions without T-DM1 were consistent with data from previous studies regarding the number of microtubules with elongating ends, the speed of elongation, and the linearity of the direction of elongation in the absence of an ADC *in vitro* [33,34]. However, the details of microtubule elongation activity in a living tumor environment have not yet been reported. Tumor vessels are irregularly arranged in tumors, resulting in an uneven localization of factors that migrate out of tumor vessels. Thus, tumors are composed of a heterogeneous group of cancer cells [26,35,36], and the expression levels of ADC target molecules on the cell membrane differ among tumor cells [37]. Additionally, microtubule elongation activity may differ among tumor cells. Notably, it is difficult to fix tumor cells and then observe their microtubule dynamics; therefore, it is important to analyze

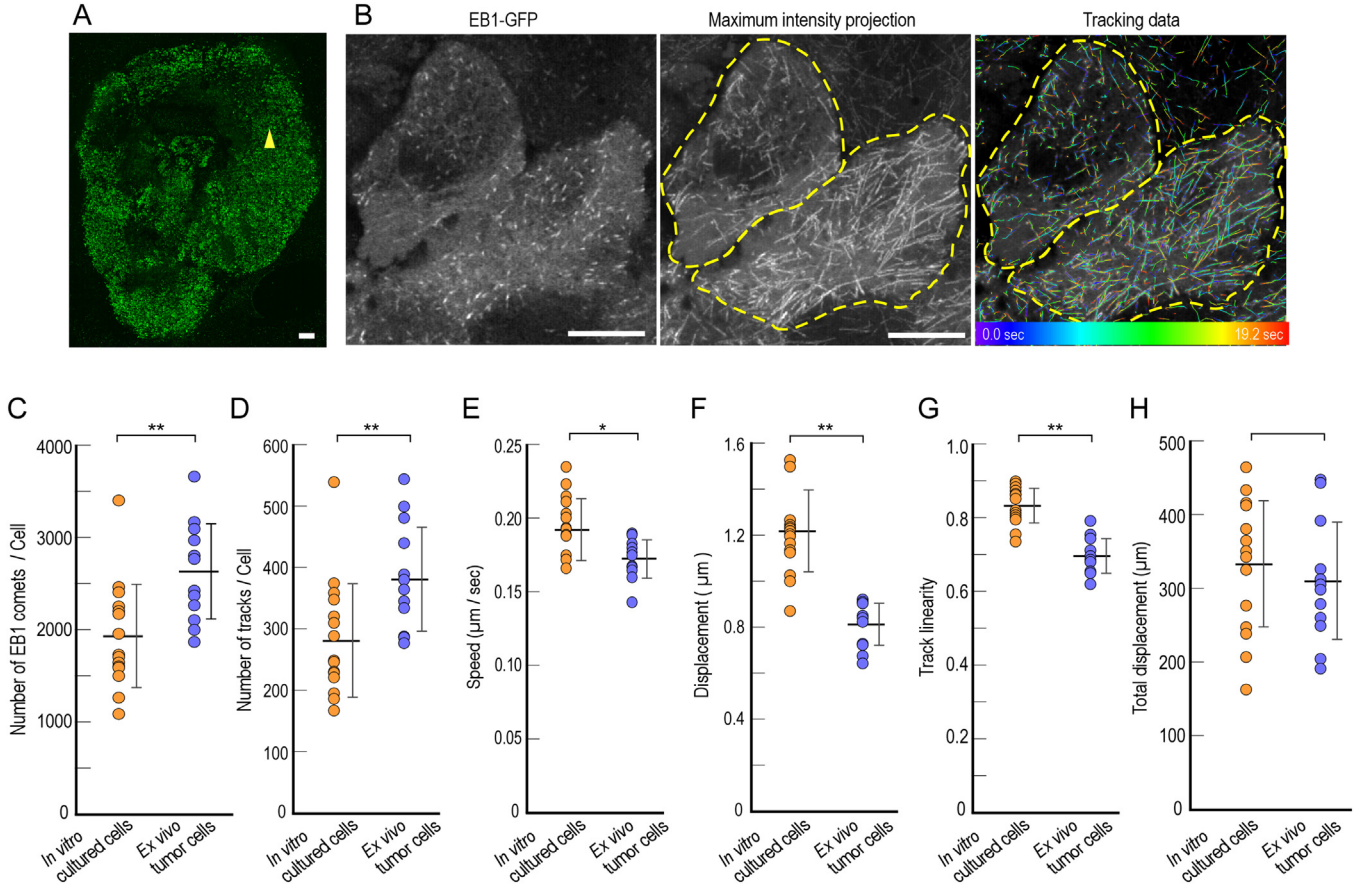

Figure 5. Imaging of microtubule elongation in living tumor cells and analysis of elongation characteristics. (A) Typical fluorescence images of 200-μm–thick living tumor tissue sections. The yellow arrowhead presents the location of B, which shows a typical image of tumor cells. Bar, 1 mm. (B) Typical fluorescence image of living tumor cells expressing EB1-EGFP. The image on the left is a still image, the image in the center is a time-lapse fluorescence image overlay, and the image on the right shows an overlay of the digital image data generated using Imaris on top of the center image. The yellow dotted line represents the outline of the cell. Bar, 10 μm. The color scale represents the location of comets at different time points. (C-H) Analysis results of EB1-EGFP comet movement in living tumor cells. EB1-EGFP comet movements tracked for ≥2 seconds during the 20-second observation period were analyzed. We arbitrarily selected 12 living tumor cells with a fluorescence intensity consistent with observed in the *in vitro* EB1-EGFP cells. We compared the characteristic values of the EB1-EGFP comet movement between the *in vitro* (orange dots) and *ex vivo* (blue dots) measurements. The orange dots are identical to the dots shown in Figure 2, *C-H*. (C) The total number of EB1-EGFP comets per cell. (D) The total number of EB1-EGFP comet tracks per cell. (E) The mean movement speed of EB1-EGFP comets per cell. (F) The mean track displacement of EB1-EGFP comets per cell. (G) The mean track linearity of EB1-EGFP comets per cell. (H) Total track displacement per cell. Black bars and error bars represent the mean values and SD, respectively, of data per cell under *in vitro* and *ex vivo* conditions (C-H). Significant differences were determined using the *t* test (*$P < 0.05$ and **$P < 0.01$). Total number of EB1-EGFP comets (C), total number of EB1-EGFP comet tracks (D), mean speed of EB1-EGFP comet (E), mean track displacement of EB1-EGFP comets (F), mean track linearity of EB1-EGFP comets (G), and total track displacement (H) of left and right cell enclosed with yellow dotted line in B are 3095 and 3170 in c, 478 and 496 in D, 0.14 μm/s and 0.18 μm/s in E, 0.64 μm and 0.90 μm in F, 0.69 and 0.79 in G, and 305.9 μm and 447.9 μm in H, respectively.

microtubule elongation in living tumor cells. Thus, we created tumor-bearing mice by xenografting EB-EGFP-KPL cells into mice and analyzed the behavior of EB1-EGFP comets in living tumor cells.

Tumors, 5-10 mm in diameter, developed over a 4- to 5-week period after xenografting EB1-EGFP-KPL cells into mice. After tumor excision, we immediately cut the tumors into 200-μm–thick sections using a Vibratome. Next, we observed the living tumor tissue sections at 37°C using fluorescence imaging with a confocal microscope. EB1-EGFP expression was observed in 50% or more of the whole tumors; however, there were regions with low EB1-EGFP expression and regions with no detectable EB1-EGFP expression due to internal necrosis (Figure 5*A*). This finding demonstrated the heterogeneity among cancer cells in tumors. We arbitrarily selected 12 tumor cells in which the fluorescence intensity of the EB1-EGFP comets was comparable to that of the *in vitro* cells and captured 20-second time-lapse images of EB1-EGFP comets in living tumor cells using the same methods described for the *in vitro* experiments. Accumulation of EB1-EGFP at the plus-ends of elongating microtubules was observed in the *ex vivo* conditions (Figure 5*B*, left image). The comets moved at a consistent speed (Supplementary Movie S5). A comparison of the overlay image containing all 20-second time-lapse fluorescence images (Figure 5*B*, middle image) and the image obtained from the bright spot tracking data of EB1-EGFP comets using Imaris (Figure 5*B*, right image) demonstrated that these results were consistent, indicating that our analysis method was valid for *ex vivo* imaging. The *ex vivo* analysis of EB1-EGFP comet movements showed that the total number of EB1-EGFP comets per cell was 2630.5 ± 516.6 (mean ± SD) over 20 seconds of continuous observation (Figure 5*C*). Of these visualized comets, the number of comets that could be tracked for ≥2 seconds was 382.2 ± 84.7 per cell (mean ± SD; Figure 5*D*). Moreover, for the comets that were tracked for ≥2 seconds, the average speed was 0.17 ± 0.01 μm/s (mean ± SD; Figure 5*E*); the average track displacement, which indicates the distance that a comet traveled from its starting point, was 0.81 ± 0.09 μm per comet (mean ± SD; Figure 5*F*); the track linearity was 0.69 ± 0.05 per comet (mean ± SD; Figure 5*G*); and the total track displacement over the 20-second tracking period was 309.3 ± 79.7 μm per cell (mean ± SD; Figure 5*H*). An analysis of the significant differences between *in vitro* and *ex vivo* EB1-EGFP comet

movements demonstrated no difference in the total track displacement per cell (Figure 5*H*). However, cancer cells in living tumor tissues have unique characteristics in terms of their microtubule dynamics. Compared to cancer cells in an *in vitro* environment, the number of microtubules with elongating plus-ends was 1.36 times higher in living tumor cells (Figure 5*C*), while the microtubule elongation speed was decreased by a factor of 0.84 (Figure 5*E*),

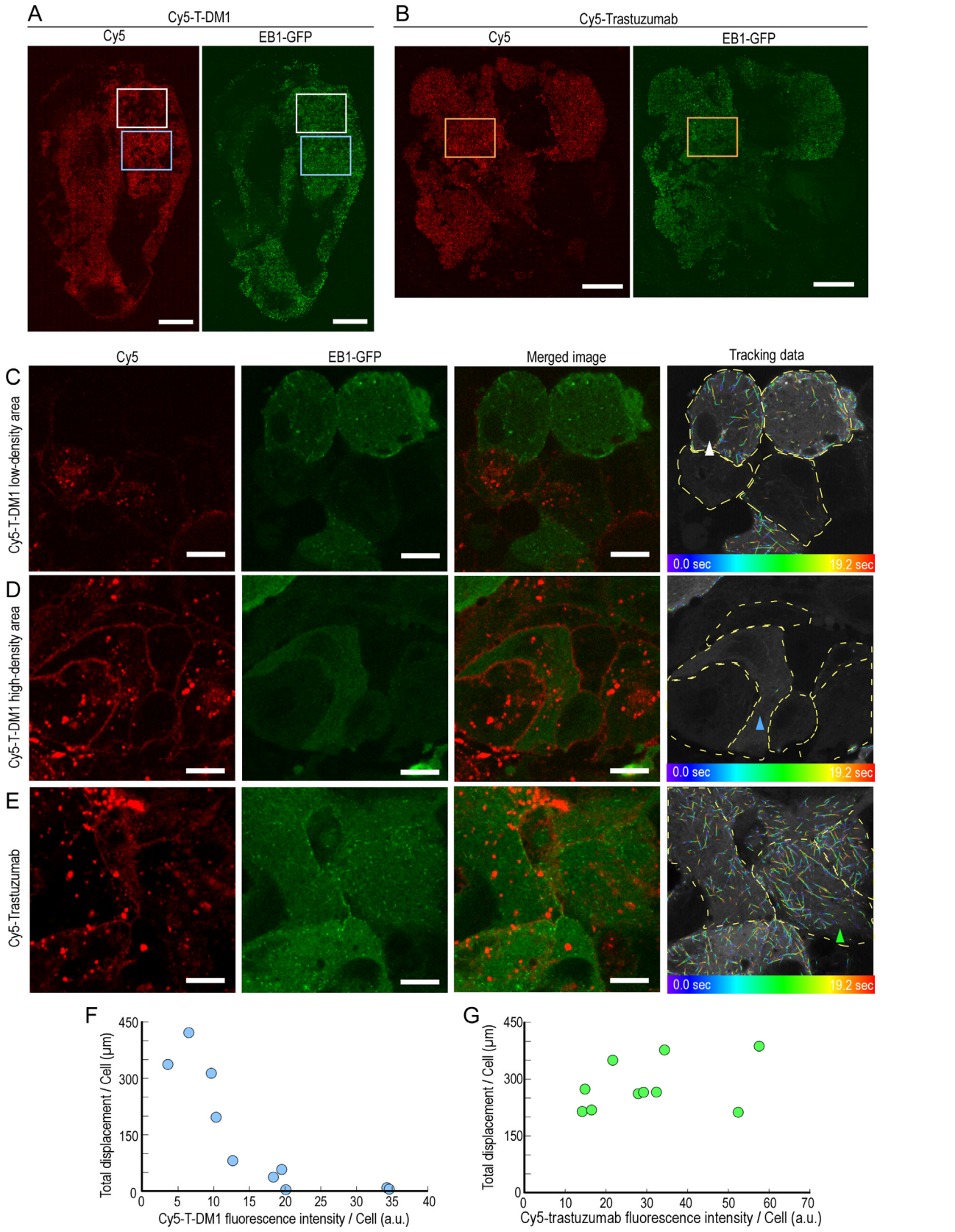

(*caption on next page*)

and the linearity of the elongation was decreased by a factor of 0.90 (Figure 5*G*). To our knowledge, this is the first to report these characteristics of microtubule elongation in living tumor cells.

Ex Vivo Imaging of Cy5-T-DM1 Drug Delivery and Microtubule Inhibition in Living Tumor Cells

To visualize T-DM1 delivery to tumors, a total of 200 μl of Cy5-T-DM1 at a concentration of 1.35 mg/ml was injected into the tail vein of mice with EB1-EGFP-KPL cell xenografts; the ratio of T-DM1 to body weight in the mice was 15 mg/kg. Twenty-four hours after the T-DM1 injection, the tumors were enucleated, and 200-μm–thick sections were prepared using a Vibratome; the sections were observed at 37°C under a confocal microscope for *ex vivo* imaging. Additionally, as a control, Cy5-labeled trastuzumab (Cy5-trastuzumab) was prepared, injected into tumor-bearing mice, and observed in the same way as the Cy5-T-DM1. Both Cy5-T-DM1 and Cy5-trastuzumab showed unequal distributions during delivery to the tumor tissue (left images in Figure 6, *A* and *B*). The EB1-EGFP expression patterns were also heterogeneous (right images in Figure 6, *A* and *B*). We quantified drug delivery and microtubule elongation inhibition simultaneously in areas of dense and sparse drug distribution in the tumor tissue. Based on the fluorescence intensities, the areas with high drug concentrations (Figure 6*A*, light blue square) had 2.2-fold higher levels of Cy5-T-DM1 in a 2500-μm^2 area than the areas with low drug concentrations (Figure 6*A*, white square). A mixture of cells was observed with varying levels of EB1-EGFP comet activity in the areas with low concentrations of Cy5-T-DM1. In areas where cells still indicated some microtubule elongation, Cy5-T-DM1 delivery to the cells was not observed (Figure 6*C*, upper two cells in the right image; the white arrowhead shows one of the two cells; Supplementary Movie S6). Conversely, Cy5-T-DM1 inhibited most of the microtubule elongation in cells in the areas of high Cy5-T-DM1 concentrations (Figure 6*D*, right image; Supplementary Movie S7).

Next, we investigated the effect of the Cy5-T-DM1 dose administered in tumor-bearing mice to the T-DM1 delivery to tumors or microtubule elongation activity in living tumor cells. The difference in the Cy5-T-DM1 dose administered increased the heterogeneity of the drug delivery to tumors (Supplementary Figure 4). In Figure 6, the ratio of Cy5-T-DM1 to mouse body weight was 15 mg/kg. In tumor-bearing mice administered 3.0 mg/kg Cy5-T-DM1, which is one fifth of 15 mg/kg, low-density areas of Cy5-T-DM1 or areas without Cy5-T-DM1 expanded (Supplementary Figure 4). Furthermore, in tumor-bearing mice administered 0.6 mg/kg Cy5-T-DM1, which is one fifth of 3.0 mg/kg, Cy5-T-DM1 was almost not delivered to most tumor cells (Supplementary Figure 4). The correlation between microtubule elongation based on measurements of EB1-EGFP comet movement and the intracellular concentration of Cy5-labeled T-DM1 in 10 arbitrarily selected cells was calculated in tumor-bearing mice administered 15 mg/kg Cy5-T-DM1; a high coefficient of correlation was observed (Figure 6*F*; Supplementary Figure 5, $R = -0.815$). These data are the first to characterize the correlation between ADC delivery and cytotoxicity in living tumor cells.

In the control experiment, an unequal distribution of Cy5-trastuzumab, similar to that of Cy5-T-DM1, was observed (Figure 6*B*), and in regions of high drug concentration (Figure 6*B*, orange square), most of the trastuzumab was localized within the tumor cells (Figure 6*E*). However, the same analysis as that used in Figure 5, *C* and *D* showed that regardless of the intracellular concentration of trastuzumab, the microtubule elongation activity was comparable to that in the T-DM1–untreated group (Figure 5; Figure 6, *E* and *G*; Supplementary Movie S8). These results demonstrated that the observed inhibition of microtubule elongation in living tumor cells induced by T-DM1 was due to the DM1 contained in the T-DM1 complex, and inhibition of microtubule elongation was due to T-DM1 uptake by cells.

Discussion

Previous studies have provided substantial information from measurements of EB1 comets in the absence of an ADC *in vitro*; however, no previous study has utilized the measurement of EB1 comet movement to evaluate microtubule elongation in living tumor cells [23,34]. Therefore, the details of microtubule elongation activity in tumor cells are poorly understood. In this study, the results of microtubule elongation analysis in living tumor cells demonstrated that the total displacement over 20 seconds in one cell was similar between *in vitro* cells and tumor cells (Figure 5*H*); however, large differences were observed in the characteristics of microtubule dynamics with regard to the total displacement in both cell types. Living tumor cells contained 1.36-fold more microtubules with an elongating plus-end than *in vitro* cells (Figure 5*C*), while the microtubule elongation speed was decreased by a factor of 0.84 (Figure 5*E*), and the linearity of elongation was decreased by a factor of 0.90 (Figure 5*G*). For microtubules under *in vitro* cell culture conditions, the flat two-dimensional environment facilitates cellular processes such as cell division and intracellular transport, and such an environment may require less microtubule three-dimensional rearrangement than a three-dimensional tumor environment [35]. Conversely, extracellular stimuli may exert greater control over cell division and intracellular transport in a three-dimensional *in vivo* environment than in an *in vitro* environment. Therefore, microtubules in living tumor cells are required to regulate their cell polarity in a three-dimensional environment, leading to microtubule elongation in a greater number of directions than in *in vitro* cells. This may contribute to an increased number of microtubules with elongating ends and a decreased linearity of microtubule tracks in living tumor cells compared to *in vitro* cells. The decreased microtubule elongation speed in living tumor cells compared to *in vitro* cells may be attributed to *in vitro* cells being present in nutrient-rich conditions and exposed to larger amounts of proteins that regulate microtubule structure and elongation speed than cells in a tumor environment, which is substantially less nutrient-rich. Therefore, *in vitro* and tumor cells measured under the same (37°C) conditions may demonstrate a difference in microtubule elongation speeds. In practice, even in cloned identical cells, cell proliferation is generally faster under *in vitro* conditions than in a tumor environment. Differences in oxygen and nutrient concentrations may lead to a difference in proliferative ability and microtubule elongation speed in the

← **Figure 6.** Correlation between the level of T-DM1 delivery and inhibition of microtubule elongation in living tumor cells. Fluorescence images of 200-μm–thick sections of living tumor tissue from tumor-bearing mice administered Cy5-T-DM1 (A) or trastuzumab (B). The white and blue squares in A represent the areas with low and high concentrations of Cy5-T-DM1, respectively. These areas are magnified in C and D, respectively. The orange squares in B represent the areas with high concentrations of Cy5-trastuzumab; a magnified view of these areas is shown in E. Bar, 1 mm (A, B). (C) Cy5-labeled T-DM1 and EB1-EGFP fluorescence in areas of low Cy5-T-DM1 delivery in living tumor cells. (D) Cy5-T-DM1 and EB1-EGFP fluorescence in areas of high Cy5-T-DM1 delivery in living tumor cells. (E) Cy5-trastuzumab and EB1-EGFP fluorescence in areas with high concentrations of Cy5-trastuzumab in living tumor cells. The leftmost images in C-E present the fluorescence of Cy5-T-DM1 or Cy5-trastuzumab. The center-left images in C-E present the fluorescence of EB1-EGFP and are still images with an exposure time of 1.07 seconds. The center-right images in C-E present still images merged with images of fluorescence from Cy5-T-DM1 or trastuzumab and EB1-EGFP. The rightmost images in C-E present the digital images that are overlays of EB1-EGFP comet movement as measured using Imaris on top of images that were created using maximum intensity projection methods to overlay all the fluorescence images of EB1-EGFP. The color scale shows the position of the comets at arbitrary points in time (C-E). The yellow dotted lines represent the cell outlines (C-E). Bar, 10 μm. (F) The correlation between the amounts of Cy5-T-DM1 delivered to tumor cells and microtubule polymerization activity (blue dots). (G) The correlation between the amounts of Cy5-trastuzumab delivered to tumor cells and microtubule polymerization activity (green dots). In C and D, Cy5-T-DM1 fluorescence intensity and total displacement/cell in the cell shown as white arrowhead in C or blue arrow in D are 9.7 a.u. and 313.1 μm or 20.1 a.u. and 2.4 μm, respectively. Similarly, Cy5-trastuzumab fluorescence intensity and total displacement/cell in the cell shown as green arrowhead in E are or 34.4 a.u. and 377.7 μm, respectively.

two different environments. Furthermore, we failed to observe a large change in the total track displacement, a unified metric for measuring microtubule elongation activity, which may be attributed to the complexity of the characteristics of microtubule elongation activity, as described above.

There has been no previous study evaluating the *in vitro* ADC efficacy as measured by changes in the EB1 comet movement. In our *in vitro* studies, inhibition of microtubule elongation by T-DM1 increased in a concentration- and reaction time–dependent manner. For example, in case of *in vitro* cells that were treated with Cy5-T-DM1 for 24 hours, the distribution of Cy5-T-DM1 fluorescence intensity on and in the cell was approximately 0.1-15.3 a.u./cell and the total track displacement was approximately 223.6-366.8 μm/cell for cells incubated with 0.001 μg/ml Cy5-T-DM1 (Figure 4*B*, blue dots). Similarly, Cy5-T-DM1 fluorescence intensity was approximately 13.6-59.6 a.u./cell and the total track displacement was approximately 83.7-162.6 μm/cell (Figure 4*B*, green dots) in the 0.01-μg/ml Cy5-T-DM1 treatment group. The Cy5-T-DM1 fluorescence intensity was approximately 34.5-93.7 a.u./cell and the displacement was 5.2-62.7 μm/cell (Figure 4*B*, yellow dots) in the 0.1-μg/ml Cy5-T-DM1 treatment group; the intensity was approximately 54.7-106.5 a.u./cell and the displacement was 0.2-52.8 μm/cell (Figure 4*B*, pink dots) in the 1.0-μg/ml Cy5-T-DM1 treatment group. From these *in vitro* data under 0.001-1.0 μg/ml Cy5-T-DM1 treatment conditions, the following relational expression was derived: $y = -3.1x + 255.8$ (Supplementary Figure 5). On the other hand, 24 hours after injecting 15 mg/kg Cy5-T-DM1 into the tail vein during the *ex vivo* experiments, the distribution of Cy5-T-DM1 fluorescence intensity on and in the tumor cell changed from approximately 3.6 to 34.2 a.u./cell in tumor cells, and in response to the change in Cy5-T-DM1 distribution, the total track displacement changed from 2.4 to approximately 421.3 μm/cell (Figure 6*F*, blue dots; Supplementary Figure 5). From the *ex vivo* data, the following relational expression was derived: $y = -12.0x + 350.4$ (Supplementary Figure 5). In a comparison of coefficients of *in vitro* and *ex vivo* relational expression, the sensitivity of *ex vivo* EB1-EGFP-KPL cells to T-DM1 was 3.9-fold higher than the *in vitro* cells ($-12.0/-3.1 \fallingdotseq 3.9$), although EB1-EGFP-KPL cells in both environments were originally identical. In other words, these data indicate that microtubule elongation may be affected by a substantially smaller change in the amount of drug delivered to the living tumor cells than to cells in an *in vitro* environment, suggesting that tumor cells are more sensitive to changes in drug concentration than *in vitro* cells. These results show that it is important to evaluate drug efficacy in living tumor cells to accurately understand the anticancer efficacy of ADCs. The concepts and methods described in this study contribute to improving the accuracy of the preclinical process for developing ADCs.

Conclusion

We developed a quantitative evaluation method at the single tumor cell level in living tumor tissue considering the heterogeneous cellular delivery and inhibitory effects of an ADC-containing microtubule inhibitor. Furthermore, the results of this study suggest that the responsiveness of T-DM1 and the dynamics of microtubule elongation activity differ between *in vitro* and *in vivo* conditions. Therefore, this method is presumed to be an effective means to measure the efficacy of ADC in a heterologous tumor microenvironment and is expected to be useful for future ADC development.

Supplementary data to this article can be found online at https://doi.org/10.1016/j.tranon.2020.100764.

Acknowledgements

We thank Y. Ishigaki for technical assistance. We also acknowledge the support of the Biomedical Research Core at the Tohoku University Graduate School of Medicine. A portion of this work was supported by a Grant-in-Aid for Challenging Exploratory Research (19K22549) from the Japan Society for the Promotion of Science (K.G.).

Author Contributions

K. G., H. N., N. F., and Y. N. conceived and designed the project and designed experiments. M. T.-K., N. K., Y. H., M. T., H. T., and T. I. contributed to the development of the concepts through discussion of this study. K. G. and H. H. created the EB1-EGFP-KPL cells. H. N., M. T.-K., and N. K. cultured cells and generated tumor-bearing mice. H. T. and T. I. prepared trastuzumab and T-DM1. H. N. and M. T.-K. performed the animal experiments. H. N. conducted the imaging experiments and obtained the data. K. G., H. N., N. F., and Y. N. analyzed the results. K. G. wrote the paper.

Declaration of Competing Interests

The authors declare that they have no conflicts of interest in relation to the contents of this article.

References

[1] A Beck, L Goetsch, C Dumontet, N Corvaia, Strategies and challenges for the next generation of antibody-drug conjugates, Nat. Rev. Drug Discov. 16 (2017) 315–337.
[2] P Polakis, Antibody drug conjugates for cancer therapy, Pharmacol. Rev. 68 (2016) 3–19.
[3] JM Lambert, RV Chari, Ado-trastuzumab Emtansine (T-DM1): an antibody-drug conjugate (ADC) for HER2-positive breast cancer, J. Med. Chem. 57 (2014) 6949–6964.
[4] PJ Carter, GA Lazar, Next generation antibody drugs: pursuit of the 'high-hanging fruit', Nat. Rev. Drug Discov. 17 (2018) 197–223.
[5] A Akhmanova, CC Hoogenraad, Microtubule plus-end-tracking proteins: mechanisms and functions, Curr. Opin. Cell Biol. 17 (2005) 47–54.
[6] BP Bouchet, A Akhmanova, Microtubules in 3D cell motility, J. Cell Sci. 130 (2017) 39–50.
[7] M Yasunaga, S Manabe, A Tsuji, M Furuta, K Ogata, Y Koga, T Saga, Y Matsumura, Development of antibody-drug conjugates using DDS and molecular imaging, Bioengineering (Basel) (2017) 4.
[8] M Ritchie, L Tchistiakova, N Scott, Implications of receptor-mediated endocytosis and intracellular trafficking dynamics in the development of antibody drug conjugates, MAbs 5 (2013) 13–21.
[9] S Xu, Internalization, trafficking, intracellular processing and actions of antibody-drug conjugates, Pharm. Res. 32 (2015) 3577–3583.
[10] GD Lewis Phillips, G Li, DL Dugger, LM Crocker, KL Parsons, E Mai, WA Blattler, JM Lambert, RV Chari, RJ Lutz, et al., Targeting HER2-positive breast cancer with trastuzumab-DM1, an antibody-cytotoxic drug conjugate, Cancer Res. **68** (2008) 9280–9290.
[11] M Barok, M Tanner, K Koninki, J Isola, Trastuzumab-DM1 causes tumour growth inhibition by mitotic catastrophe in trastuzumab-resistant breast cancer cells in vivo, Breast Cancer Res. 13 (2011) R46.
[12] J Black, G Menderes, S Bellone, CL Schwab, E Bonazzoli, F Ferrari, F Predolini, C De Haydu, E Cocco, N Buza, et al., SYD985, a novel duocarmycin-based HER2-targeting antibody-drug conjugate, shows antitumor activity in uterine serous carcinoma with HER2/Neu expression, Mol. Cancer Ther. **15** (2016) 1900–1909.
[13] G Menderes, E Bonazzoli, S Bellone, J Black, G Altwerger, A Masserdotti, F Pettinella, L Zammataro, N Buza, P Hui, et al., SYD985, a novel duocarmycin-based HER2-targeting antibody-drug conjugate, shows promising antitumor activity in epithelial ovarian carcinoma with HER2/Neu expression, Gynecol. Oncol. **146** (2017) 179–186.
[14] S Verma, D Miles, L Gianni, IE Krop, M Welslau, J Baselga, M Pegram, DY Oh, V Dieras, E Guardino, et al., Trastuzumab emtansine for HER2-positive advanced breast cancer, N. Engl. J. Med. **367** (2012) 1783–1791.
[15] PC Thuss-Patience, MA Shah, A Ohtsu, E Van Cutsem, JA Ajani, H Castro, W Mansoor, HC Chung, G Bodoky, K Shitara, et al., Trastuzumab emtansine versus taxane use for previously treated HER2-positive locally advanced or metastatic gastric or gastro-oesophageal junction adenocarcinoma (GATSBY): an international randomised, open-label, adaptive, phase 2/3 study, Lancet Oncol. **18** (2017) 640–653.
[16] H Wang, W Wang, Y Xu, Y Yang, X Chen, H Quan, L Lou, Aberrant intracellular metabolism of T-DM1 confers T-DM1 resistance in human epidermal growth factor receptor 2-positive gastric cancer cells, Cancer Sci. 108 (2017) 1458–1468.
[17] JR Conway, NO Carragher, P Timpson, Developments in preclinical cancer imaging: innovating the discovery of therapeutics, Nat. Rev. Cancer 14 (2014) 314–328.
[18] M de Jong, J Essers, WM van Weerden, Imaging preclinical tumour models: improving translational power, Nat. Rev. Cancer 14 (2014) 481–493.
[19] MA Miller, R Weissleder, Imaging of anticancer drug action in single cells, Nat. Rev. Cancer 17 (2017) 399–414.
[20] JD Orth, RH Kohler, F Foijer, PK Sorger, R Weissleder, TJ Mitchison, Analysis of mitosis and antimitotic drug responses in tumors by in vivo microscopy and single-cell pharmacodynamics, Cancer Res. 71 (2011) 4608–4616.
[21] SJ Sahl, SW Hell, S Jakobs, Fluorescence nanoscopy in cell biology, Nat. Rev. Mol. Cell Biol. 18 (2017) 685–701.
[22] GM Thurber, KS Yang, T Reiner, RH Kohler, P Sorger, T Mitchison, R Weissleder, Single-cell and subcellular pharmacokinetic imaging allows insight into drug action in vivo, Nat. Commun. 4 (2013) 1504.
[23] M Borowiak, W Nahaboo, M Reynders, K Nekolla, P Jalinot, J Hasserodt, M Rehberg, M Delattre, S Zahler, A Vollmar, et al., Photoswitchable inhibitors of microtubule dynamics optically control mitosis and cell death, Cell 162 (2015) 403–411.

[24] MA Jordan, L Wilson, Microtubules as a target for anticancer drugs, Nat. Rev. Cancer 4 (2004) 253–265.
[25] A Akhmanova, MO Steinmetz, Tracking the ends: a dynamic protein network controls the fate of microtubule tips, Nat. Rev. Mol. Cell Biol. 9 (2008) 309–322.
[26] JH Baker, KE Lindquist, LA Huxham, AH Kyle, JT Sy, AI Minchinton, Direct visualization of heterogeneous extravascular distribution of trastuzumab in human epidermal growth factor receptor type 2 overexpressing xenografts, Clin. Cancer Res. 14 (2008) 2171–2179.
[27] C Cilliers, H Guo, J Liao, N Christodolu, GM Thurber, Multiscale modeling of antibody-drug conjugates: connecting tissue and cellular distribution to whole animal pharmacokinetics and potential implications for efficacy, AAPS J. 18 (2016) 1117–1130.
[28] I Fuso Nerini, L Morosi, M Zucchetti, A Ballerini, R Giavazzi, M D'Incalci, Intratumor heterogeneity and its impact on drug distribution and sensitivity, Clin. Pharmacol. Ther. 96 (2014) 224–238.
[29] B Vitre, FM Coquelle, C Heichette, C Garnier, D Chretien, I Arnal, EB1 regulates microtubule dynamics and tubulin sheet closure in vitro, Nat. Cell Biol. 10 (2008) 415–421.
[30] P Bieling, S Kandels-Lewis, IA Telley, J van Dijk, C Janke, T Surrey, CLIP-170 tracks growing microtubule ends by dynamically recognizing composite EB1/tubulin-binding sites, J. Cell Biol. 183 (2008) 1223–1233.
[31] J Kurebayashi, S Yamamoto, T Otsuki, H Sonoo, Medroxyprogesterone acetate inhibits interleukin 6 secretion from KPL-4 human breast cancer cells both in vitro and in vivo: a possible mechanism of the anticachectic effect, Br. J. Cancer 79 (1999) 631–636.
[32] Y Ogitani, T Aida, K Hagihara, J Yamaguchi, C Ishii, N Harada, M Soma, H Okamoto, M Oitate, S Arakawa, et al., DS-8201a, a novel HER2-targeting ADC with a novel DNA topoisomerase I inhibitor, demonstrates a promising antitumor efficacy with differentiation from T-DM1, Clin. Cancer Res. **22** (2016) 5097–5108.
[33] Y Mimori-Kiyosue, N Shiina, S Tsukita, The dynamic behavior of the APC-binding protein EB1 on the distal ends of microtubules, Curr. Biol. 10 (2000) 865–868.
[34] A Matov, K Applegate, P Kumar, C Thoma, W Krek, G Danuser, T Wittmann, Analysis of microtubule dynamic instability using a plus-end growth marker, Nat. Methods 7 (2010) 761–768.
[35] HG Augustin, GY Koh, Organotypic vasculature: from descriptive heterogeneity to functional pathophysiology, Science (2017) 357.
[36] HJ Lee, AN Seo, EJ Kim, MH Jang, KJ Suh, HS Ryu, YJ Kim, JH Kim, SA Im, G Gong, et al., HER2 heterogeneity affects trastuzumab responses and survival in patients with HER2-positive metastatic breast cancer, Am. J. Clin. Pathol. **142** (2014) 755–766.
[37] SR Adams, HC Yang, EN Savariar, J Aguilera, JL Crisp, KA Jones, MA Whitney, SM Lippman, EE Cohen, RY Tsien, et al., Anti-tubulin drugs conjugated to anti-ErbB antibodies selectively radiosensitize, Nat. Commun. 7 (2016) 13019.